Free-carrier effects in GaAs single modulation-doped quantum well as applied to active Q-switching of injection lasers

V. Kalinovsky, T. Shubina, I. Shvechikov, A. Toropov

Free-carrier effects in GaAs single modulation-doped quantum well as applied to active Q-switching of injection lasers

V. S. Kalinovsky, T. V. Shubina, I. Yu. Shvechikov and A. A. Toropov

A. F. Ioffe Physico-Technical Institute, Academy of Sciences, 26 Politekhnicheskaya, 194021 St. Petersburg, Russia

Abstract. — Free carrier effects in a modulation-doped GaAs QW placed in the n-region of a p-n junction were successfully used to obtain active Q-switching in a two-section GaAs/AlGaAs DH laser structure. The modulator section uses the blue shift of the QW absorption edge due to band filling by a 2D electron gas whose concentration could be controlled between 0 and 8×10^{11} cm^{-2} by external bias voltage. Only about 100 mV of the modulating voltage was necessary to provide stable active Q-switching. The threshold injection current density ranged from 400 to 800 A/cm^2. The modulation bandwidth is estimated to be not less than 4-5 GHz. A simple electrostatic model is suggested to describe electrooptical phenomena in a modulation-doped QW which underlie the operation of the device.

1. Introduction.

Active Q-switching is a very attractive method to control laser generation and to produce ultrashort optical pulses because lower modulation power is required than, for example, for gain switching. This is usually attained in a two-segment laser consisting of an optical amplifier and an electroabsorption loss modulator. The amplifier is driven by injection current while the modulator uses some electrooptical effect and is controlled by an external bias voltage. Different electrooptical phenomena have been utilized to provide convenient operation of the devices. These are the Franz-Keldysh effect in a double heterostructure [1] and the quantum confined Stark Effect (QCSE) in a multiquantum well laser structure [2]. There is one common problem in utilizing these effects. There is noticeable absorption even in the most transparent state of the modulator at the wavelength corresponding to the generation of a modulator-free laser. This seems to be the reason for increased threshold current of the two-segment laser [3]. An increase in the electric field applied to the modulator active region results in additional enhancement of absorption below the band gap. This occurs due to both the shape alteration of the band edge caused by the Franz-Keldysh effect and the red shift of the excitonic peak due to the QCSE.

To solve this problem, we propose to use free carrier effects in a modulation-doped QW, in particular, the blue shift of the QW absorption edge due to the band filling by 2D electron gas [4, 5]. The latter is very similar to the Moss-Burstein effect in doped bulk semiconductors. Free electrons present in an n-modulation-doped QW fill in the lowest confined states up to the Fermi level. For 2D gas of electrons of mass m_e, the Fermi energy E_F is equal to $(\pi \hbar/m_e) \times N_s$ where N_s is the sheet concentration. In GaAs, for example, E_F is about 35 meV when $N_s = 1 \times 10^{12}$ cm^{-2}. Light absorption can be associated only with the transitions to unoccupied electronic states. So, one may expect the absorption edge to be shifted towards higher energies than in an undoped QW and the energy shift $\Delta E = (1 + m_e/m_h) E_F$ is proportional to N_s. This allows in principal to reduce the modulator losses and, hence the injection current density of the two-segment laser. For this purpose we used an AlGaAs/GaAs p-n laser heterostructure with an undoped GaAs single QW placed near the p-n junction in the n-doped region. The advantage of this structure is that it allows to control the electron population in the QW by applying the bias voltage to the p-n junction. To elucidate the voltage dependence of N_s and electrooptical characteristics of the structure, spectral studies were made of the photocurrent and the waveguide light transmission. Efficient active Q-switching was obtained and studied in two-segment lasers fabricated from the structures.

2. Samples and spectral waveguide technique.

The structures under study were grown by MBE and low-temperature LPE and were designed to operate as a laser and comprised a single-mode waveguide. The threshold injection current density ranged from 200 to 500 A/cm^2. The paper describes mainly an MBE structure as the others demonstrated a similar behaviour.

Figure 1 shows a schematic view of the structure. An undoped GaAs QW was put in the centre of a 0.4 μm wide $Al_{0.28}Ga_{0.72}As$ optical waveguide n-doped up to 1.3×10^{17} cm^3. The width of the QW was intended to be 110-120 Å by the growth process, which was confirmed by TEM measurements and additionally checked using luminescence spectra of an analogous structure with an undoped QW grown under the same conditions. The waveguide was surrounded by $Al_{0.48}Ga_{0.52}As$ confining layers. An abrupt asymmetric p-n junction was formed at the interface between the waveguide and the p-doped upper confining layer.

The slab waveguide geometry of the samples was used to study the waveguide light
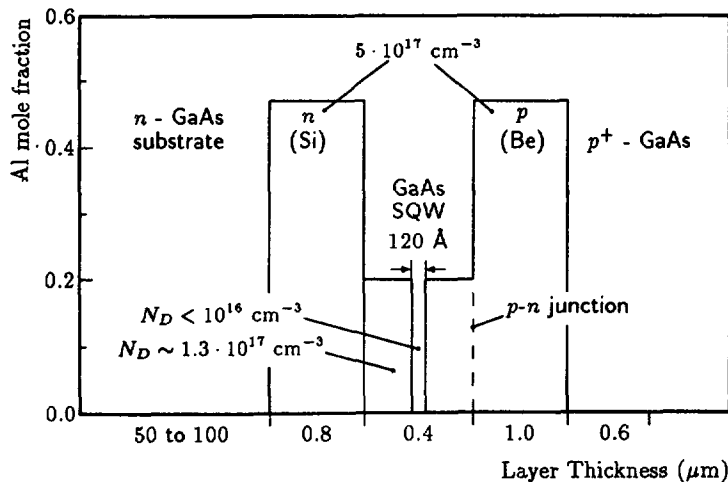

Fig. 1. — Schematic view of a modulation-doped QW structure.

transmission. The emission of an iodine tungsten lamp transmitted through a monochromator and polarizer was focused with a fine 60^x microobjective in a 2 μm strip onto a slab guide sample placed between two gold contacts. That gave excitation of the principal mode, which was the only mode for a 0.4 μm waveguide with the given content of Al in the barriers.

The emission from the sample was collected with a microscope and sensed with a photomultiplier. The technique allowed to measure the spectra of absorption, electroabsorption, and photocurrent selectively for the TE and TM waveguide modes.

3. Electrooptical characteristics of QW waveguide structures.

The 2D electron gas present in the QW is supposed to be responsible for the electrooptical characteristics, so it is important to know the dependence of its concentration N_s on the external bias. For this purpose the photocurrent was measured as a function of the reverse bias in a sample long enough (about 400 μm) to absorb practically all the photons above the QW absorption band edge. So, the photocurrent was almost independent of the absorption coefficient and reflected the extension of the space depletion regions (SDRs) in the structure.

There were three depletion regions in the structure : one on each side of the QW and one more is the p-n junction SDR (see Fig. 2). The photocurrent was measured as a function of the
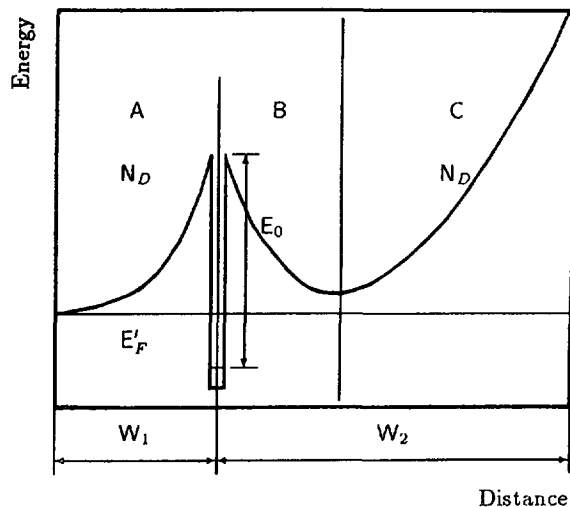

Fig. 2. — Schematic diagram of the potential and space depletion regions (A, B, C) in the structure. W_2 is the distance from the QW to the p-n junction interface. N_D is the n-region doping level.

reverse bias voltage at two different wavelengths. The first wavelength is chosen above the GaAs QW band edge but below the band edge of the AlGaAs waveguide. That provided the registration of the photocurrent from the QW only. The photocurrent ($I_{ph_{QW}}$) is plotted in figure 3 against the reverse bias voltage. It increases rapidly up to 2 V and saturates above this value. It seems likely that the reverse bias produces the extension of the p-n junction SDR which overlaps completely with one of the two QW depletion regions at about 2 V. At this voltage almost all the photoexcited carriers are separated and its further increase can no more increase the photocurrent.

In the second measurement the light wavelength was chosen above the band gap of the AlGaAs waveguide, so it was a non-guided operation. In this case the photocurrent is the sum

of the values from the QW and waveguide material in the SDRs. The voltage dependence of this total photocurrent (I_{ph_w}) is shown in figure 3. The curve has three portions. Below 2 V the photocurrent increases rapidly, which corresponds to the convergence of the SDRs. At higher voltage the QW photocurrent becomes saturated and further increase is due only to the enhancement of photocurrent from the waveguide SDRs. But the p-n junction SDR and one of the two QW SDRs are completely overlapped and the enhancement is proportional to the extension of the other QW SDR. Whilst there is 2D electron gas in the QW it screens the potential and prevents the extension of this region. Therefore, the photocurrent is almost voltage-independent until the full depletion of the QW occurs at about 4 V. After that the photocurrent varies with voltage as in a simple p-n junction.
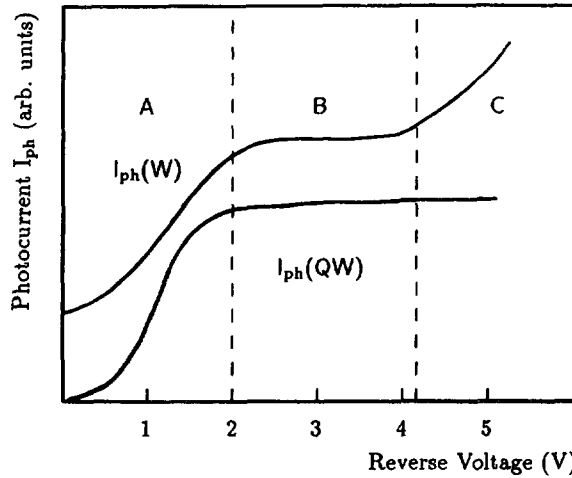

Fig. 3. — Photocurrent as a function of the reverse bias V_r : $(I_{ph_{QW}})$, photocurrent from the QW ; (I_{ph_w}), photocurrent from the waveguide.

To describe the details of this process, it is necessary to solve self-consistently the Poisson and Schrödinger equations. For the structures under consideration, the QW width is small compared to the width of the SDRs, so one can neglect the QW shape alteration and the Stark shift of the confined levels. With this assumption the photocurrent data can be interpreted in the framework of a simple electrostatic model. The model also implies that the SDRs of the p-n junction and the QW are fully overlapped and the photocurrent increase is proportional to the extension of the other QW SDR (region (A) in Fig. 2). Besides, the electron Fermi level is supposed to be fixed throughtout the sample. The Poisson equation solved with these assumptions gives the following expressions for the voltage V_0 of complete depletion of the QW, sheet electron concentration N_s and the width of the QW depletion region W_1 :

$$V_0(E_0) = \frac{(W_2 \sqrt{eN_D} + \sqrt{2 E_0 \varepsilon})^2}{2 \varepsilon} \tag{1}$$

For $V > V_0 N_s = 0$ and

$$W_1(V) = \sqrt{\frac{2 \varepsilon V}{eN_D}} - W_2 . \tag{2}$$

For $V < V_0$,

$$N_s(V) = \frac{N_D[W_1(V) + W_2]^2}{2\,W_2} - \frac{\varepsilon V}{eW_2} \tag{3}$$

and

$$W_1(V) = \frac{\sqrt{f(V, E_0)} - AeN_D\,W_2}{eN_D\left(\dfrac{e}{\varepsilon}\,W_2 + A\right)} \tag{4}$$

where

$$f(V, E_0) = 2\,eN_D\left(\frac{e}{\varepsilon}\,W_2 + A\right)(E_0\,W_{2e} + A\varepsilon V) - \frac{e^3\,W_2^3\,N_D^2\,A}{\varepsilon} \tag{5}$$

Here e, ε and V denote, respectively, the elementary charge, the permittivity and the total voltage $(V = V_r + V_{\text{built-in}})$; V_r is the reverse bias voltage; A is given by $\pi\hbar^2/m_e$. The parameters W_2, E_0, N_D are explained in figure 2.

Assuming the photocurrent to be proportional to $W_1(V)$ one can express its voltage dependence as

$$I_{\text{ph}}(V) = \frac{C}{\sqrt{N_D}}\sqrt{\frac{2\,\varepsilon}{e}}\,(\sqrt{V} - \sqrt{V_0}) \tag{6}$$

for $V > V_0$, and for $V < V_0$

$$I_{\text{ph}}(V) = \frac{C}{\sqrt{N_D}} \times \frac{\sqrt{f(V)} - \sqrt{f(V_0)}}{e\left(\dfrac{e}{\varepsilon}\,W_2 + A\right)} \tag{7}$$

Here C is an adjustable parameter.

These dependences, joined together at the point $V = V_0$, are plotted in figure 4. They show good agreement with the experimental data, which proves the validity of the simplified
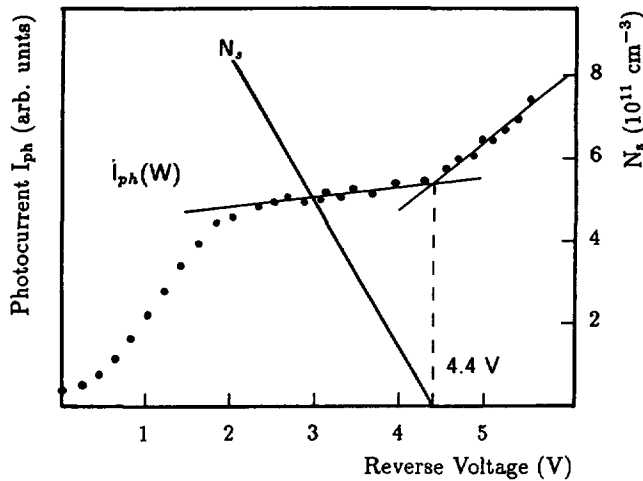

Fig. 4. — Photocurrent I_{ph_W} and 2D electron gas concentration N_s as a function of the reverse bias V_r. Circles : experimental points. Solid line : calculation.

description. The calculated voltage dependence of N_s is also shown in figure 4. The increase in the bias from 2 to 4.4 V decreases N_s from 8×10^{11} cm^{-2} to zero.

The high value of N_s predicts a significant blue shift of the absorption edge associated with the optical transitions from the lowest hole states to the lowest electron level in the QW due to the band filling. To detect this phenomenon the spectra of the waveguide absorption for the TE and TM waveguide modes were measured at different bias voltages at room temperature.

The spectra in figure 5 demonstrate discernible absorption peaks. An increase in the reverse bias changes significantly the band edge shape. First of all, there is a noticeable enhancement of absorption in the whole spectral region of the band edge. Then there is an insignificant shift of the peaks. Finally, we observe the appearance and a large red shift of a specific *wave* of
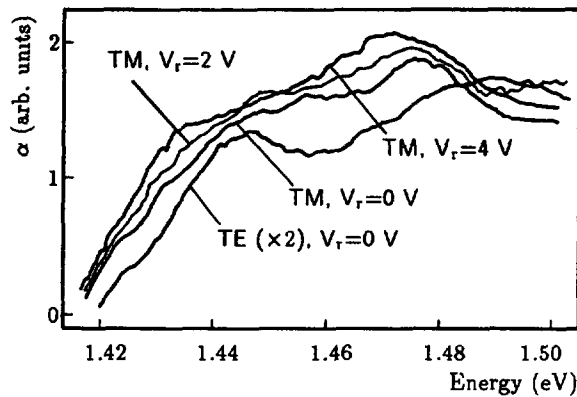

Fig. 5. — Absorption spectra of the TE and TM waveguide modes.

absorption above 2 V of reverse the bias. The last feature can be clearly seen in the differential electromodulation spectra of transmission measured at different constant voltages (see Fig. 6). The specific resonance-shape differential spectrum, which includes regions of increasing and decreasing absorption (positive and negative signal), appears at about 2 V, shifts approximately by 50 meV without significant increase in the spectral width and then disappears gradually above 4 V.

Figure 7 shows the energy position of the spectral singularities as a function of the bias. The characteristic energy of the *rapidly* shifted resonance is determined as a zero of the
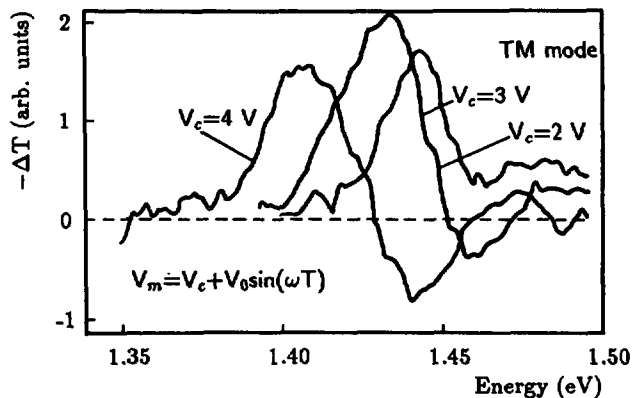

Fig. 6. — Differential electromodulation transmission spectra of the TM mode.
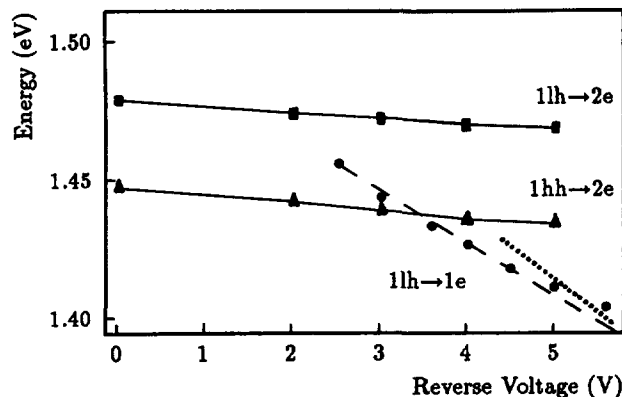
Fig. 7. — Energy position of the spectral singularities against the reverse bias. Position of the « slowly » shifted peaks of the TE (triangles) and TM (squares) waveguide modes. Position of the « rapidly » shifted singularity of the TM mode absorption (full circles). Broken line — the computation for the Moss-Burstein shift based on the photocurrent data (the slope $\Delta E/\Delta V_r = 18.3$ meV/V) ; dotted line — computation of 1 lh → 1 e interband transition. (See text).

electromodulation spectra. The singularities can be divided into two types according to their dependence on the voltage. There are *slowly* shifted absorption peaks for the TE and TM waveguide modes and the *rapidly* shifted resonance observed in both polarizations. The total shift is about 6 meV for the *slowly* shifted peaks and about 50 meV for the *rapidly* shifted resonance.

It is very likely that the lowest spectral singularity corresponds to the lowest possible optical transition in the QW. We mean the transition between the lowest hole and electron states, when there is no electron gas in the QW, and the transition from the lowest hole state to above the Fermi edge when there is 2D electron gas of a concentration N_s in the QW. One can check this assumption comparing the slope of the experimental dependence with that estimated for the Moss-Burstein shift, using the data of the photocurrent measurements. The calculated line plotted in figure 7 is adjusted to the experimental one at the point of the lowest voltage. The agreement is rather good at high N_s, but there is some divergence at low electron concentration.

When the well becomes completely depleted at the bias voltage in excess of 4.4 V, the potential profile of the QW bottom becomes close to triangular. It is very likely that the positions of the lower levels in such a well are close to that of an analogous undoped well under relevant electric field which can be estimated using (1) and (2) (the bias voltage of 4.4 V corresponds to $E = 1 \times 10^5$ V/cm).

To verify this assumption we have computed the energies of the first electron and light hole levels in a 120 Å GaAs QW sandwiched between $Al_{0.28}Ga_{0.72}As$ barriers in the electric field range concerned. The calculations have been carried out by numerical treatment of the one-dimensional Schrödinger equation with transformed variables to give differential equation with Airy function solutions [6]. The calculated dependence of the interband transition energy between the two levels on the bias voltage across the sample for $V > 4.4$ V is shown in figure 7 as a dotted line. The value of 6 meV have been used for the exciton binding energy. Within the accuracy of the experimental measurement of the position of the spectral singularity, the calculated and measured dependences are in close agreement.

There is a number of other electrooptical effects in a modulation-doped QW. For example, the band gap renormalization occurs due to the many-body effect, which leads to the band gap

shrinkage. This phenomenon must be predominant at relatively low electron concentration [5]. Then, quenching of the excitonic absorption must be due to screening [7, 8]. Apparently, it is this phenomenon that increases the absorption observed in the spectral region close to the band edge. One can also expect a certain Stark shift of the confined levels. Besides, the band mixing in the QW is supposed to be significant, because the optical transitions occur in a modulation-doped QW when the wave vector **k** is equal to the Fermi value rather than to zero, as in an undoped QW. This causes mixing of the light and heavy hole states and breaks the selection rules for the TE and TM waveguide polarizations. This suggestion can explain well the same spectral position of the lowest resonance and good separation of higher light and heavy hole states for the TE and TM waveguide modes. These states seem to provide smooth peaks in the absorption spectra due to the « forbidden » optical transitions 1 hh → 2 e for the TE mode and 1 lh → 2 e for the TM mode, which become allowed in the skewed QW. An insignificant voltage-induced shift of the peaks results mainly from the Stark shift of the confined levels.

A comparison has been made of the band edge shift measurements and the computation of the Moss-Burstein shift using the photocurrent data. This comparison confirms the domination of the blue absorption band edge shift due to the electron band filling over the effects of the band gap renormalization and the Stark shift which were assumed to be small or compensate each other in the region of N_s higher than $\sim 3 \times 10^{11}$ cm^{-2}. Together with the excitonic absorption quenching, the blue shift produces a singificant electromodulation of absorption in the spectral range of about 60 meV around the band edge, and it is just this characteristic that gives rise to efficient active Q-switching in the low-threshold two-segment laser.

4. Two segment laser operation.

Figure 8 shows a schematic structure of a fabricated two-segment ridge laser. The ridge waveguide was chemically etched to a width of 12 μm. SiO$_2$ was used to confine the current injection to the ridge. The sections are electrically isolated and optically interconnected by a common waveguide. The electrical isolation of about 100 kΩ results from the 4 μm wide separation selectively etched between the segments.

The spectral width of efficient electrooptical modulation provided by free carrier effects is
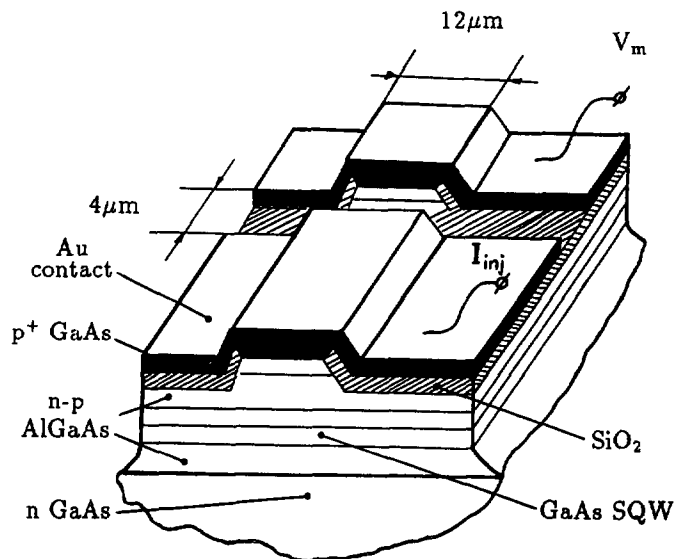

Fig. 8. — Schematic view of the two-segment ridge laser.

large enough to overlap even the electroluminescence region of the structure. That allows to test the modulation ability of the two segment structure in a small-signal electroluminescence operation, when the amplifier section is driven by current, much lower than the laser threshold current. Figure 9a shows the intensity of the light-emission-diode radiation passed through the modulator and measured as a function of the reverse bias. This dependence again reflects the specific points 2 V and 4 V, which correspond respectively to the full overlap of the QW and the p-n junction SDRs and to the complete depletion of the QW. These values set up the limits for the voltage region of efficient electromodulation. They result only from the geometrical size and doping level and can be calculated before growing the structure. The structure under discussion is very suitable to study the electrooptical behaviour, while for the device application it is more convenient to shift the electromodulation region to the zero voltage. This idea has been realized in a similar structure. The modulation depth of the electroluminescence emission is about 75 % for a 150 μm long modulator. So, the device is rather effective even in the light emission diode operation.

The threshold current density of the lasers with the modulator section of about 100 μm in length ranged from 400 to 800 A/cm² for the most transparent state of the modulator. The threshold current can be almost trebled by applying the DC bias to the modulator. In the active Q-switching operation the optical amplifier is driven by a continuous current, while a microwave signal is applied to the modulator. The DC bias can also be applied to the modulator if it is necessary to obtain efficient modulation. Only about 100 mV of the
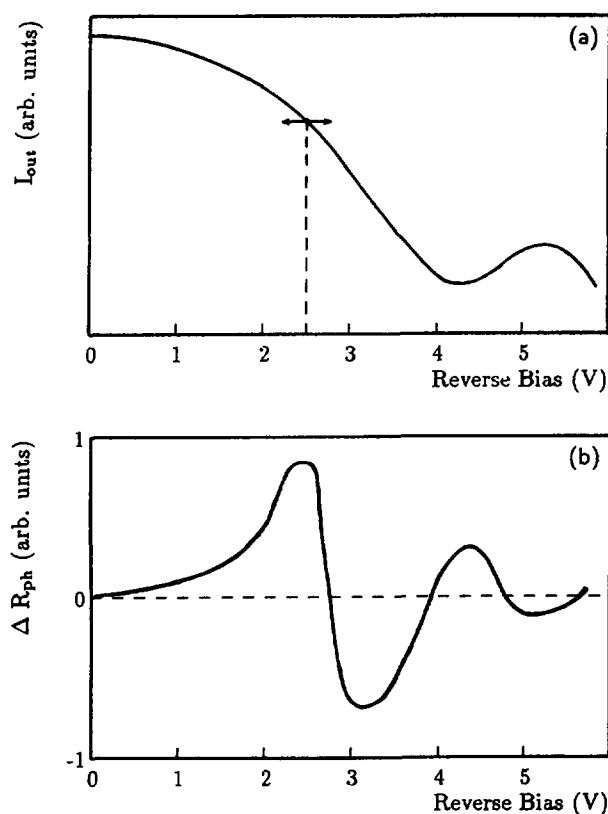

Fig. 9. — Small-signal characteristics of the modulator. The modulator output (a) and differential response (b) against the reverse bias.

modulating voltage is necessary to provide stable Q-switching, so that every period of the microwave signal gives rise to a single optical laser pulse. The most important parameters of the laser generation are the pulsewidth and the attainable repetition rate. When the laser is long enough, the pulsewidth is limited by the entire laser cavity rather than by the modulator characteristics. The time dependence of the long laser generation is shown in figure 10. The total length of the laser cavity was 830 μm. The dependence was obtained using a p-i-n photodiode with time resolution of about 50 ps. The pulsewith of about 160 ps and the upper limit of the repetition rate about 1.5 GHz seem to be determined by the dynamic characteristics of the entire laser cavity. For the 250 μm laser the pulsewidth is about 50 ps and seems to be limited by the photodetector time response. The repetition rate in this case is about 3 GHz and is very likely to be limited by the modulator frequency characteristics.
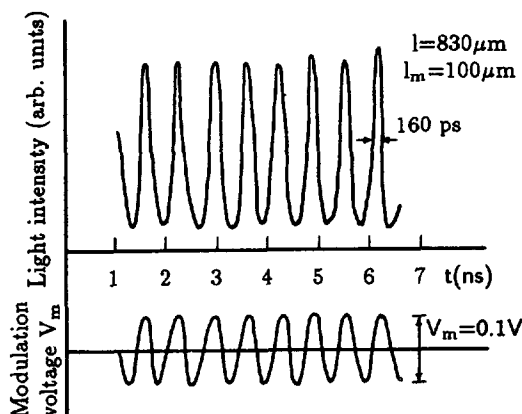

Fig. 10. — Time response of the long laser operated by a 100 mV microwave signal.

It seems interesting to compare our data with that of Arakawa *et al.* [2] concerning active Q-swithing in two-segment laser realized with the quantum confined Stark shift. The reported repetition rate of the device ranged from 100 MHz to 3.2 GHz and a pulse FWHM $\Delta\tau_{1/2}$ of 18.6 ps. However, the threshold current density was much higher (several kA/cm^2 as results from the data presented in the paper).

5. High-frequency characteristics of the modulator.

Special measurements were made to find the frequency characteristics of the modulator in small-signal operation. The two-segment structures were used. The amplifier was pumped with relatively low current to prevent the laser generation in the system, which was, however, high enough to provide a probe light signal to be detected after passing through the modulator. A special technique was developed to achieve high time resolution of a small electroluminescence signal. For this, the signficant intrinsic nonlinearity of the modulator electrooptical response was used. The nonlinear character of the dependence of the output light intensity on the bias voltage (see Fig. 9a) allows to raise the sensitivity by conventional lock-in technique and a relatively slow photoelectron multiplier used as a light detector, while the frequency band of the set is determined by that of the modulator.

Applying a constant reverse voltage to the modulator we can change the output light signal according to the curve in figure 9a. Superposition of the microwave sinus signal on the constant bias V_0 gives rise to a periodic output light signal. However, no change occurs in the registered signal, provided the V_0 is located within the linear portion of the modulator

electrooptical response curve. This is due to application of the slow photomultiplier which integrates a high frequency signal. However, shifting the V_0 to the nonlinear portion of the curve increases or decreases the registered signal with respect to the level of the output signal when there is no microwave modulation (differential response), so that the latter reflects the nonlinearity of the modulator electrooptical response. Thus, by varying the V_0 and the microwave signal frequency one can measure the frequency response of the modulator.

In figure 9b the differential response measured at constant frequency is plotted against V_0. It can easily be seen that the curve corresponds to the electrooptical modulator response. Figure 11 exhibits the frequency dependence of the response at constant V_0 corresponding to the extremum near 2.5 V. This dependence reflects the frequency bandwidth of the modulator and well accounts for the limitation on the repetition rate of the short laser Q-switching. The region of the efficient modulation extends approximately up to 3 GHz.
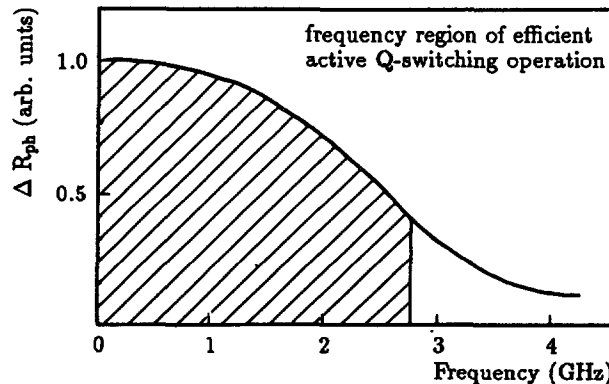

Fig. 11. — Frequency dependence of the differential response at about 2.5 V of the DC reverse bias on the modulator.

The high frequency characteristics of the device are determined by the rate of electron tunnelling through the QW barrier, provided the dimensions and, hence, the capacitance of the device are small enough. The rate is a function of the barrier height and width, which depend on the device design. The frequency characteristics can be improved through increasing the doping level, which lessens the barrier width and height, increasing the tunnelling rate. However, the problem arises to meet two requirements : the modulator design providing high frequency characteristics and low threshold laser operation. The preliminary estimation shows the possibility of low threshold operation within the frequency band of about 5 GHz.

6. Conclusion.

We have presented and discussed the measurements of electrooptical characteristics of a waveguide laser structure with a modulation-doped QW. It has been shown that the observed free carrier effects are very convenient to obtain efficient active Q-switching of a two-segment laser with very low threshold current density. The active Q-switching is achieved at the threshold current density as low as 400-800 A/cm^2 depending on the modulator length. Only 100 mV of the modulating microwave signal is needed to provide active Q-switching and to obtain optical pulses less than 50 ps wide with the repetition rate up to 3 GHz. It has been demonstrated that the frequency bandwidth of the short laser operation is determined by the high frequency characteristics of the modulator rather than by the dynamic features of the whole laser cavity.

Acknowledgments.

References

[1] TSANG D. Z., WALPONE J. N., LIAU J. L., GROVES S. H., DIADIUK V., *Appl. Phys. Lett.* **45** (3) (1984) 204-206.

[2] ARAKAWA Y., LARSON A., PASLASKI J., YARIV A., *Appl. Phys. Lett.* **48** (9) (1986) 561-563.

[3] TARUCHA S., OKAMOTO H., *Appl. Phys. Lett.* **48** (1) (1986) 1-3.

[4] LIVESCU G., MILLER D. A. B., CHEMLA D. S., RAMASWANG M., CHANG T. Y., SAUER N., GOSSARD A. C., ENGLISH J. H., *IEEE J. Quantum Electron.* **24** (8) (1988) 1677-1689.

[5] BAR JOSEPH I., KUO J. M., KLINGSHIRN C., LIVESCU G., CHANG T. Y., MILLER D. A. B., CHEMLA D. S., *Phys. Rev. Lett.* **59** (1987) 1357.

[6] AUSTIN E. J., JAROS M., *Phys. Rev. B* **31** (1985) 5569-5572.

[7] SAKAKI H., YOSHIMURA H., MATSUSUE T., *Jpn J. Appl. Phys.* **26** (1987) 1104.

[8] TOMBLING C., STALLARD M. M., ROBERTS J. S., *Semicond. Sci. Technol.* **5** (1990) 502-507.